remote sensing

Article

Multi-Year Behavioral Observations of Quasi-2-Day Wave Activity in High-Latitude Mohe (52.5°N, 122.3°E) and Middle-Latitude Wuhan (30.5°N, 114.6°E) Using Meteor Radars

Liang Tang [1], Sheng-Yang Gu [2,*], Ruidi Sun [2] and Xiankang Dou [2]

[1] School of Optoelectronic Engineering, Chongqing University of Posts and Telecommunications, Chongqing 400065, China
[2] Electronic Information School, Wuhan University, Wuhan 430072, China; sunruidi@whu.edu.cn (R.S.)
* Correspondence: gushengyang@whu.edu.cn

Abstract: The behavior of multi-year quasi-2-day wave (Q2DW) activity in the high and middle latitudes in the mesosphere and lower thermosphere regions during 2013–2022 is revealed, for the first time, using two meteor radars along the 120°E longitude, which are located at Mohe (52.5°N, 122.3°E) and Wuhan (30.5°N, 114.6°E). We first describe the interannual monthly mean characteristics of the Mohe and Wuhan winds. We then determine the extraction of the Q2DWs via a least-squares method and calculate the occurrence dates, amplitudes, periods, and phases of the zonal and meridional Q2DWs. We find that the summer zonal wind speed of Mohe reached ~35 m/s at ~94 km in 2022, and the meridional wind speed reached ~−20 m/s at ~88 km in 2017. Similarly, the zonal and meridional wind speeds in Wuhan reached ~48 m/s and ~−30 m/s at ~94 km and ~90 km, respectively, in the summer of 2020. Statistical analysis shows that, in Mohe and Wuhan, the highest frequency of Q2DWs is observed between days 200 and 220. The Q2DW is mainly associated with the background mean wind and is consistent with a selective filtering mechanism. We believe that the correlation between wind shear and Q2DW amplitude is higher in summer because wind shear reaches its maximum when Q2DW starts to amplify. The wave period of the Mohe zonal Q2DW is longer than that of the Wuhan zonal Q2DW, while that of the meridional Q2DW is shorter. In addition, the zonal and meridional Q2DW amplitudes are weaker in Mohe than in Wuhan. The vertical wavelength of the Q2DW in Wuhan is shorter than that in Mohe. Solar activity F10.7 does not appear to be strongly correlated with Q2DW behavior in Mohe and Wuhan.

Keywords: Q2DW; high and middle latitude difference; statistical analysis; meteor radars

check for updates

Citation: Tang, L.; Gu, S.-Y.; Sun, R.; Dou, X. Multi-Year Behavioral Observations of Quasi-2-Day Wave Activity in High-Latitude Mohe (52.5°N, 122.3°E) and Middle-Latitude Wuhan (30.5°N, 114.6°E) Using Meteor Radars. *Remote Sens.* **2024**, *16*, 311. https://doi.org/10.3390/rs16020311

Academic Editor: Dimitris Kaskaoutis

Received: 2 November 2023
Revised: 15 December 2023
Accepted: 8 January 2024
Published: 12 January 2024

1. Introduction

The mesosphere and lower thermosphere (MLT) are transitional regions connecting the lower and upper atmosphere. Quasi-2-day waves (Q2DWs) are global-scale atmospheric oscillations that play a crucial role in the dynamics of the MLT [1–5]. Atmospheric waves induce horizontal and vertical couplings that critically affect momentum, energy, and chemical transport throughout the atmosphere.

Recently, numerous studies have reported observations of MLT planetary waves with various durations, including quasi-2-day [6–10], 4-day [11–18], 10-day [19,20], and 16-day [21–25] waves. Ground-based radar observations have been extensively used by researchers to investigate the characteristics of these planetary waves. Muller [26] discovered significant Q2DW oscillations with a period of about 51 h using Sheffield meteoric wind radar data. Furthermore, Q2DWs have been identified at high latitudes as well as near the equator [2,4]. Mid-latitude Q2DWs exhibit distinct summer maxima characterized by one or several bursts, each lasting multiple weeks [1,3], whereas high-latitude Q2DWs demonstrate maximum activity during winter [27–32].

Long-term mean amplitudes calculated by Lilienthal and Jacobi using very-high-frequency (VHF) meteor radar data from 82 to 97 km over Collm (51°N, 13°E) from September 2004 to August 2014 exhibited pronounced summer maxima and comparatively weaker winter maxima [2]. During the summer, the meridional amplitude slightly exceeds the zonal amplitude, reaching approximately 15 m/s at 91 km altitude. There is a potential correlation between the Q2DW amplitude and background wind shear during the strong summer burst, with the Q2DW period varying between 43 and 52 h. It is important to note that there is considerable interannual variability in the Q2DW amplitudes. Gu [6] investigated long-term variations in Q2DW utilizing mesosphere horizontal winds measured via a medium-frequency radar located at Kauai, Hawaii (22°N, 160°W), from 1991 to 2006. They found that Q2DWs are amplified twice per year over Hawaii; the January event most likely represents the zonal wavenumber 3 mode, while the July event corresponds to the wavenumber 4 mode.

Ma [33] analyzed the response of Q2DWs within the MLT region to the sudden stratospheric warming that occurred in 2013. Their study is based on a meteor radar chain along the 120°E meridian in the Northern Hemisphere, which consists of four sites: Mohe (52.5°N, 122.3°E), Beijing (40.3°N, 116.2°E), Wuhan (30.5°N, 114.6°E), and Sanya (18.3°N, 109.6°E). They observed that during the sudden stratospheric warming event, low latitudes experienced a significant amplification of Q2DWs, accompanied by a clear reversal of the zonal wind direction from east to west. Liu [4] found that Q2DW can approach significant amplitudes between ±20° latitudes in the equatorial region, although they are often observed at high latitudes, and that Q2DW has the greatest variation in wave amplitude near the equator, indicating the strongest wave activity.

Previous studies have focused more on the observation results of single-station meteor radars, primarily analyzing behavioral changes in Q2DWs at mid-latitudes; however, less research has been conducted on the relationship between background wind and Q2DWs at mid-latitudes and high latitudes. The effect of background wind on Q2DW behavior varies between mid-latitudes and high latitudes, warranting further analysis using multi-site meteor radar data. In this study, the latitudinal difference in Q2DW activity in the MLT region during 2013–2022 is studied by examining the wind observation data of two meteor radar chains located at 52.5°N and 30.5°N on the ~120°E meridian in China (Mohe and Wuhan). The occurrence date and wave period of Q2DWs, as well as the amplitude difference (zonal and meridional winds), at the two stations, are calculated. Our goal is to enhance our comprehension of the behavioral characteristics of Q2DWs in Mohe and Wuhan. Section 2 briefly describes the data and analysis methods. The analytical results are presented in Section 3. Section 4 is devoted to the propagation properties of Q2DWs and the effect of F10.7 on Q2DW amplification. The conclusions are presented in Section 5.

2. Data and Analysis

The China Meridian Engineering Meteor Radar Chain (120°E) consists of four radar stations and was established by the Institute of Geology and Geophysics (IGGCAS) of the Chinese Academy of Sciences. The four observatories of the meteor radar chain range from high to low latitudes in the Northern Hemisphere; Mohe (52.5°N, 122.3°E), Beijing (40.3°N, 116.2°E), Wuhan (30.5°N, 114.6°E), and Sanya (18.3°N, 109.6°E) are located along the 120°E meridian. Zonal and meridional wind retrievals based on meteor radar observations in the altitude range of ~70–110 km have a vertical resolution of ~2 km and a temporal resolution of ~1 h. The meteor radars at the Mohe and Wuhan stations operate at 38.9 MHz with a maximum power of 20 kW and 7.5 kW, respectively. The high-latitude meteor radar at Mohe station can detect about 13,000 meteors per day, while the mid-latitude meteor radar at Wuhan station can detect about 4000–5000 [34,35]. The Mohe and Wuhan radars are conventional Atmospheric Radar System (ATRAD) meteor detection radars [36–38]. Meteor radar transmission and reception use one pair of cross dipoles and five pairs of cross dipoles, respectively. In this study, we present a statistical analysis of the characteristics of the Q2DWs at the two stations and a comparative analysis of the differences between the Q2DWs at high and middle latitudes, based on the zonal and meridional wind data between ~80 and 100 km at Mohe and Wuhan stations from 2013 to 2022, as illustrated in Figure 1. These wind data are widely used to detect changes in atmospheric activity [39–42]. Many recent studies have demonstrated the feasibility of using meteor radar data. Zonal and meridional wind data from meteor radar sites are published at the National Space Science Data Center, National Science and Technology Infrastructure of China (https://www.nssdc.ac.cn, accessed on 1 November 2023). Meteor radars can continuously measure MLT neutral winds at one location (latitude and longitude) by measuring the radial Doppler shift in radio pulses reflected from an ionized meteor trajectory near an altitude of ~90 km. At certain altitudes, the meteor count rate is sometimes very low, resulting in missing meteor radar observations and gaps in the data.

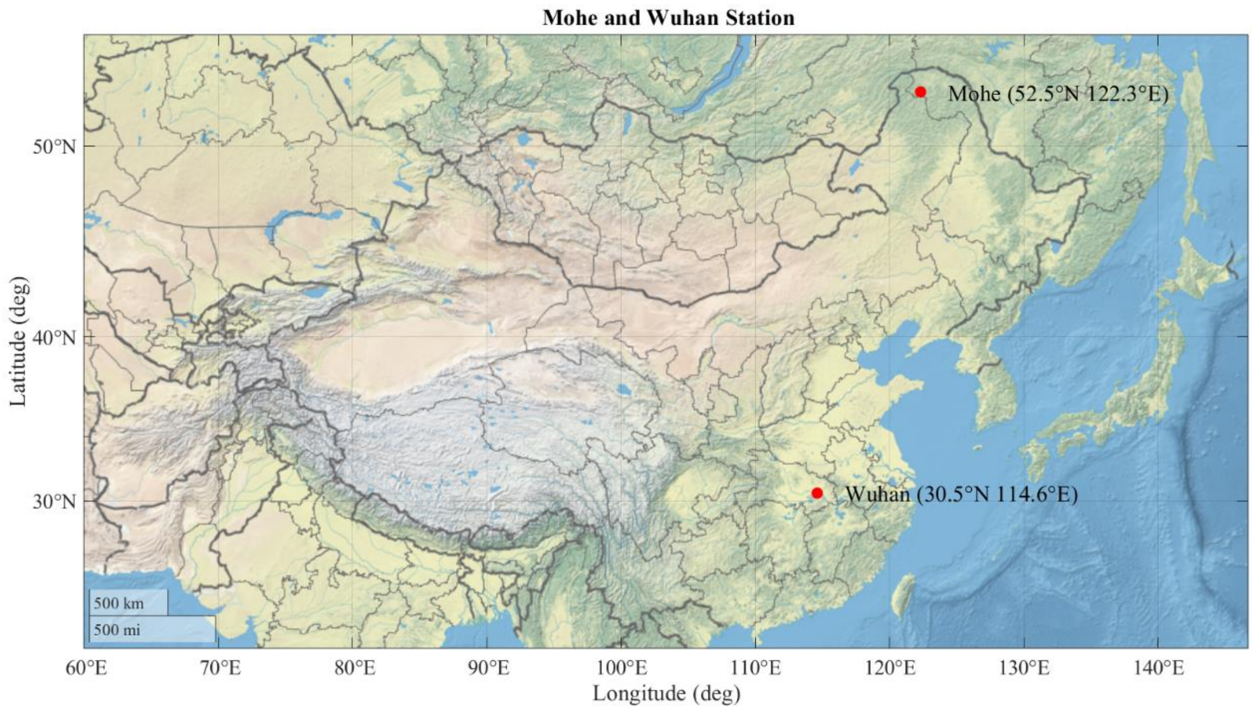

Figure 1. Location of the IGGCAS meteor radar chain at the high and middle latitudes in the Northern Hemisphere around the 120°E meridian. The two stations of the chain are Mohe (52.5°N, 122.3°E) and Wuhan (30.5°N, 114.6°E). Map information is derived from Matlab 2022b Mapping Toolbox.

To extract zonal and meridional Q2DWs, we apply the least-squares method to each time window (10 days) and then use the time window to determine the amplitude [6]. The amplitudes and phases of the Q2DW were determined through the least-squares fit applied to the zonal and meridional hourly winds, encompassing the tidal oscillations with periods of 24, 12, and 8 h, as well as the individual period of the Q2DW identified from periodogram analysis of both zonal and meridional winds. Tidal components were removed by filtering out oscillations with periods of 24, 12, and 8 h; subsequently, residuals were smoothed using two days to enhance clarity in detecting the Q2DW signal. Each fitting procedure was based on 10 days of hourly mean winds. This method has been shown to successfully identify planetary waves from meteor radar measurements [43]. In addition, we use a time window (10 days data) in our analysis, focusing on waves with periods ranging from ~36 to 60 h, with a step of 1 h. The maxima of the zonal and meridional Q2DW events are at ~90 km. Zonal and meridional Q2DW events were extracted from wind datasets measured during 2013–2022 via the Mohe and Wuhan meteor radars.

$$y = A\cos(2\pi \cdot \sigma \cdot t) + B\sin(2\pi \cdot \sigma \cdot t) + C \quad (1)$$

The values of A, B, and C in Formula (1) were obtained via least-square fitting. The frequency and Universal Time (UT) are represented using σ and t. Planetary wave amplitude R can be expressed using $R = \sqrt{A^2 + B^2}$.

$$\varnothing = \tan^{-1}\left(\frac{B}{A}\right) \tag{2}$$

In Formula (2), $\varnothing$ is the phase of the Q2DWs. A vertical wavelength is the height at which a wave travels vertically over a complete period. Therefore, the vertical wavelength can be calculated from the phase slope of Q2DWs at different altitudes.

3. Results

The temporal variability in Q2DWs at Mohe and Wuhan stations during the summer season was analyzed using hourly mean zonal and meridional winds. We only consider Q2DW because it is an important fluctuation in the MLT region. By applying the least-squares fitting method discussed in Section 2, the amplitude of the Q2DW is estimated at altitudes of ~86 km, ~90 km, and ~94 km. The diurnal variations in the Q2DW amplitudes at Mohe and Wuhan stations are shown in Figure 2a–c, g–k, b–f, and h,i as zonal and meridional components, respectively. For both components, the amplitude of the Q2DW's appearance increases with altitude, but the amplitude of the meridional component is larger than that of the zonal component. The zonal and meridional Q2DW mean amplitudes at Mohe station are the largest at ~90 km, with amplitudes of ~10 m/s and ~14 m/s, respectively. Similarly, the amplitudes at Wuhan station are about ~12 m/s and ~18 m/s at ~90 km, where the Q2DW amplitudes of both components reach their maximum. Since the focus of this study is on the latitudinal differences in the activity of Q2DWs in the MLT region and improving the understanding of the Q2DW characteristics at the two stations, we primarily analyze the Q2DW events at Mohe and Wuhan stations at ~90 km.

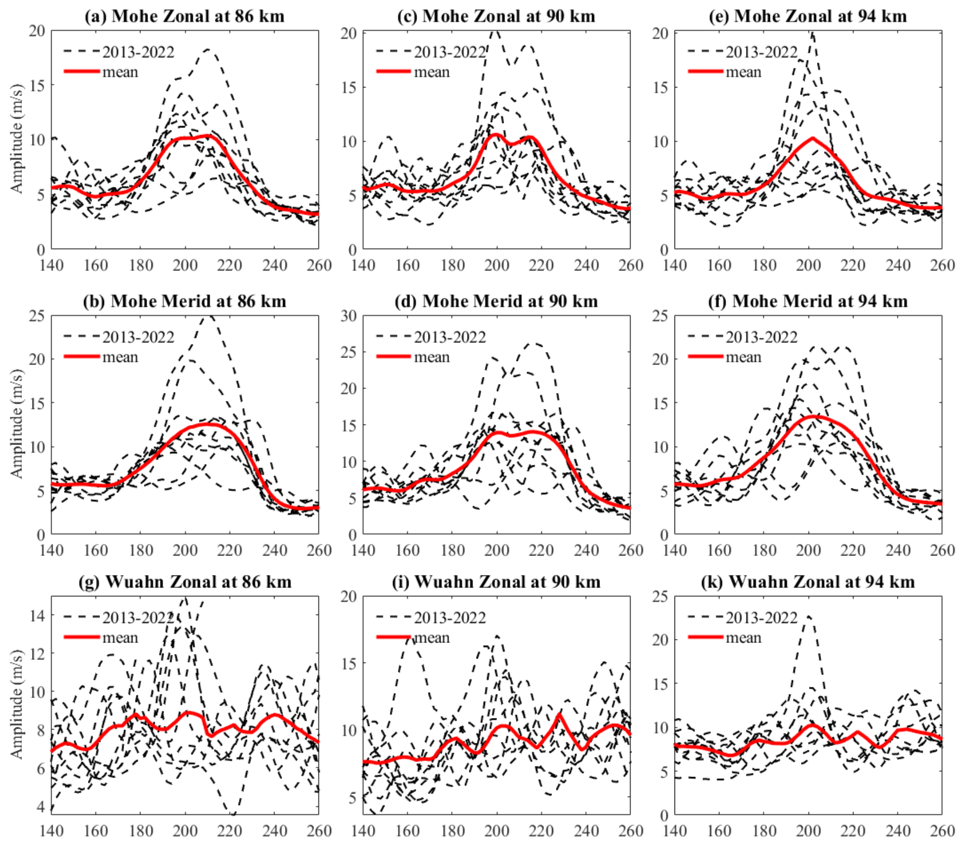

Figure 2. *Cont.*

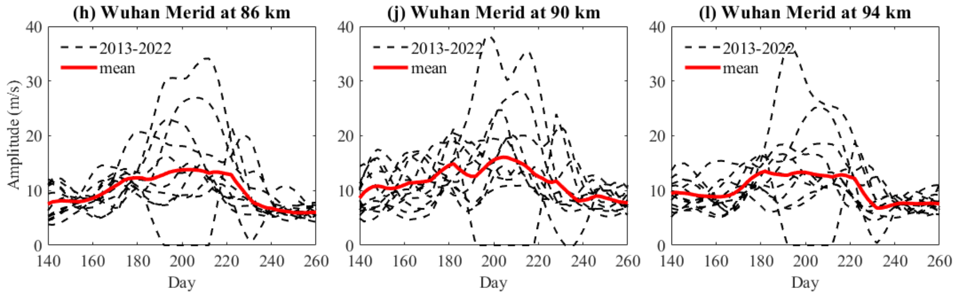

Figure 2. Time series of the mean zonal and meridional (merid) wind Q2DW amplitude at 86, 90, and 94 km altitudes over Mohe and Wuhan from 2013 to 2022.

3.1. Mean Winds

Figure 3 shows the time–height cross-sections of zonal and meridional winds observed via the meteor radar at Mohe station during 2013–2022. Here, the black line encircles data lost due to hardware and software problems with the Mohe meteor radar. The 10-year mean zonal and meridional winds are shown in Figure 3a,b. The observed zonal wind structure generally agrees with the zonal wind climatology observed via the satellite, as shown in Figure 3a. During summer (June–August), eastward winds (westward winds) are dominant below (above) ~90 km, creating strong vertical wind shear. In contrast, from October to February, relatively weak vertical wind shear is observed under strong westward winds. The monthly average strongest zonal westward wind is above ~94 km and ~30 m/s in July. Below ~84 km, the monthly average eastward winds are strongest in March, reaching ~−15 m/s. The average zonal (westward) winds are strongest in July 2016 and 2022, at about 35 m/s, while the average zonal (eastward) winds are strongest in April 2017, at about −28 m/s. From Figure 3b, it can be observed that in June–August, northward winds almost dominate at ~80–100 km. In contrast, from October to February, relatively weak vertical wind shear is observed under weak southward winds. The monthly average strongest meridional northward wind is above ~90 km, reaching ~−18 m/s in June. Above ~90 km, the monthly average southward winds are strongest in October, reaching up to ~6 m/s. The average meridional wind (northward wind) was the strongest in June 2018, at about −22 m/s, and the average meridional wind (southward wind) was the strongest in January 2015, at about 15 m/s.

From Figure 4a, it can be observed that during summer (April–August), eastward winds (westward winds) are dominant below (above) ~84 km, creating weak vertical wind shear. In contrast, strong vertical wind shear is observed from February to June under strong eastward winds. The mean monthly zonal winds are above ~94 km, with the strongest monthly westward winds around 40 m/s in July. Below ~84 km, the monthly average eastward winds are strongest in March, reaching ~−10 m/s. The average zonal (westward) winds are strongest in July 2017 and 2020, at about 47 m/s, while the average zonal (eastward) winds are strongest in March 2021, at about −15 m/s. From Figure 4b, it can be seen that from March to October, northward winds almost dominate at ~80–100 km. In contrast, the southward winds are weaker from November to February. The mean monthly meridional winds are above ~90 km, and the mean monthly northward winds are strongest in July, at about −15 m/s. Below ~84 km, the monthly average southward winds are strongest in November, reaching up to ~5 m/s. The average meridional wind (northward wind) was the strongest in October 2017, at about −30 m/s, and the average meridional wind (southward wind) was the strongest in October 2019, at about 12 m/s.

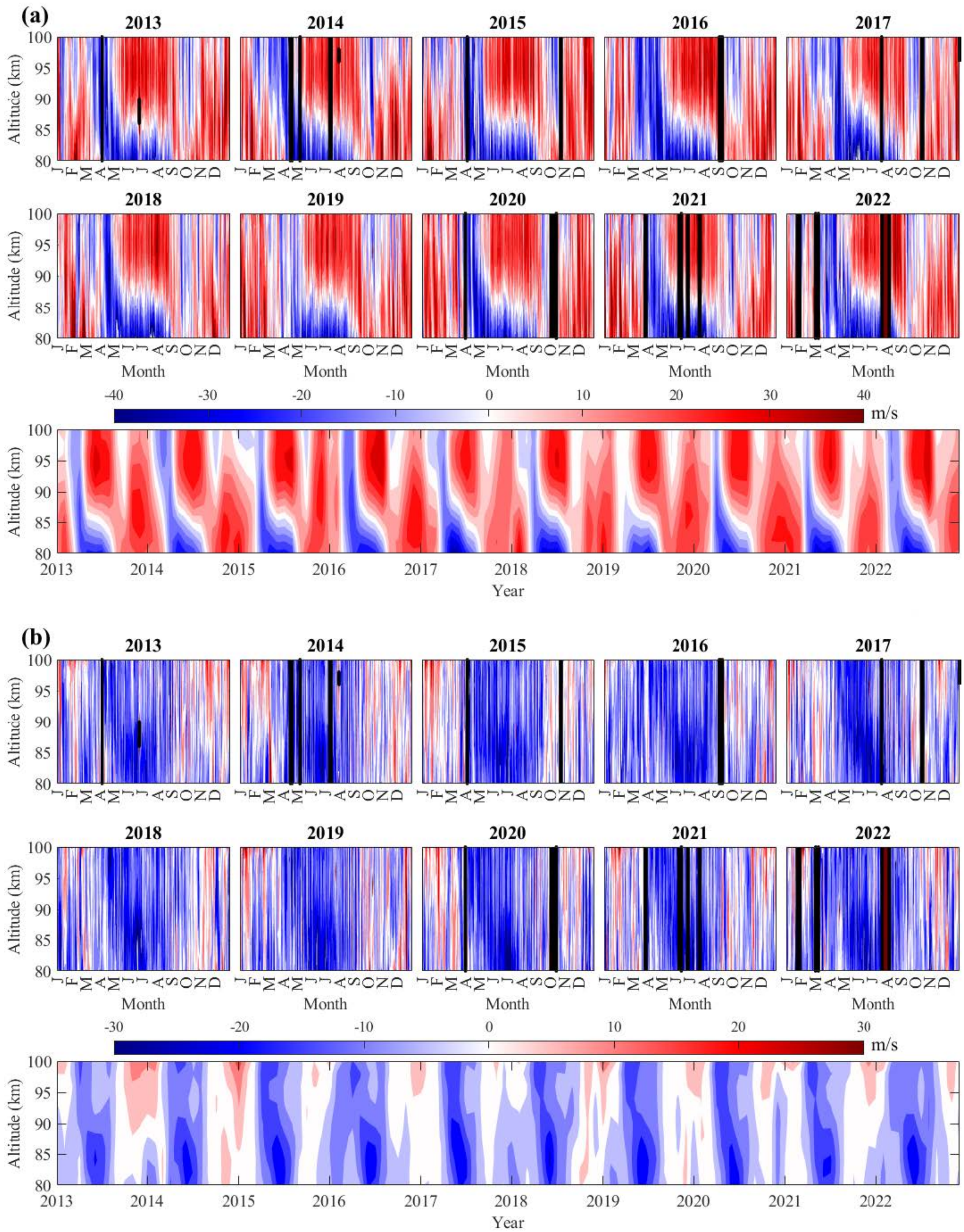

Figure 3. Time–height cross-sections of the (**a**) daily averaged and monthly averaged zonal winds observed from the meteor radar at Mohe during 2013–2022. (**b**) is the same as (**a**), but represents meridional winds. Areas surrounded by black lines represent missing data.

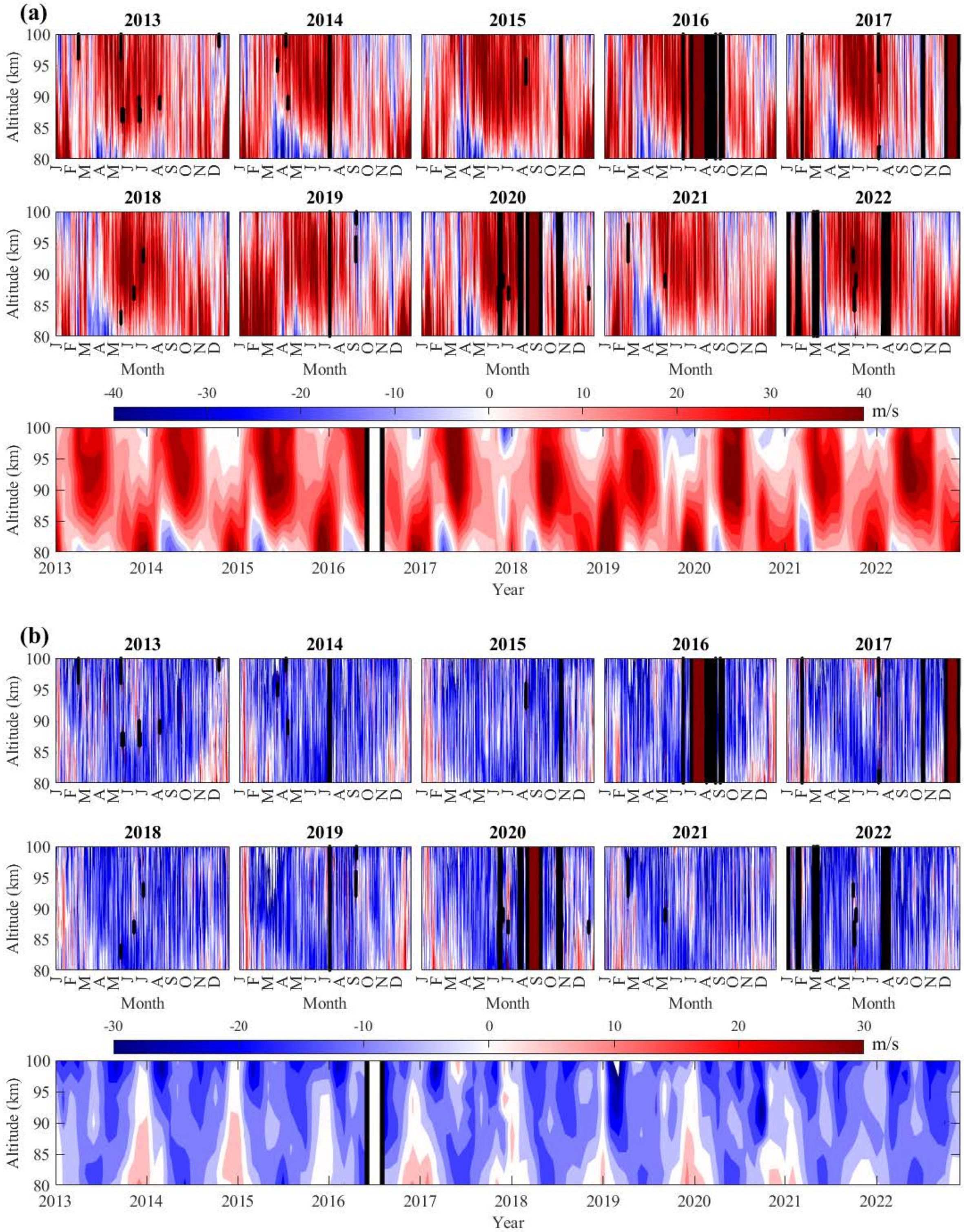

Figure 4. Time–height cross-sections of the (**a**) daily averaged and monthly averaged zonal winds observed from the meteor radar at Wuhan during 2013–2022. (**b**) is the same as (**a**), but represents meridional winds. Areas surrounded by black lines represent missing data.

3.2. Mohe Q2DW

Figure 5a,d show the averaged period–date spectra of Q2DWs at ~90 km for zonal and meridional winds from the 2014 summer. The zonal Q2DW reaches its summer maximum with an amplitude of ~18 m/s at ~50 h during days 202–211, as shown in Figure 5a.

Similarly, meridional Q2DW reaches a maximum amplitude of ~25 m/s at ~52 h during days 214–223 (Figure 5d). From Figure 5b, it can be observed that the maximum amplitude of the zonal Q2DW at ~90 km has a period of ~50 h and reaches an amplitude of ~18 m/s. Figure 5e shows the meridional Q2DW amplitude, which peaks at ~92 km at ~52 h with a maximum of ~25 m/s. The phase and amplitude of the Q2DW events are shown in Figure 5c,f. The vertical wavelength of the Q2DWs is calculated as the slope of the phase. The ~50 h Q2DW phase of the zonal wind shown in Figure 5c does not tilt much with altitude (height), resulting in an extremely long vertical wavelength (at ~150 km), whereas the vertical wavelength of the meridional ~52 h Q2DW is estimated at ~86 km (Figure 5f).

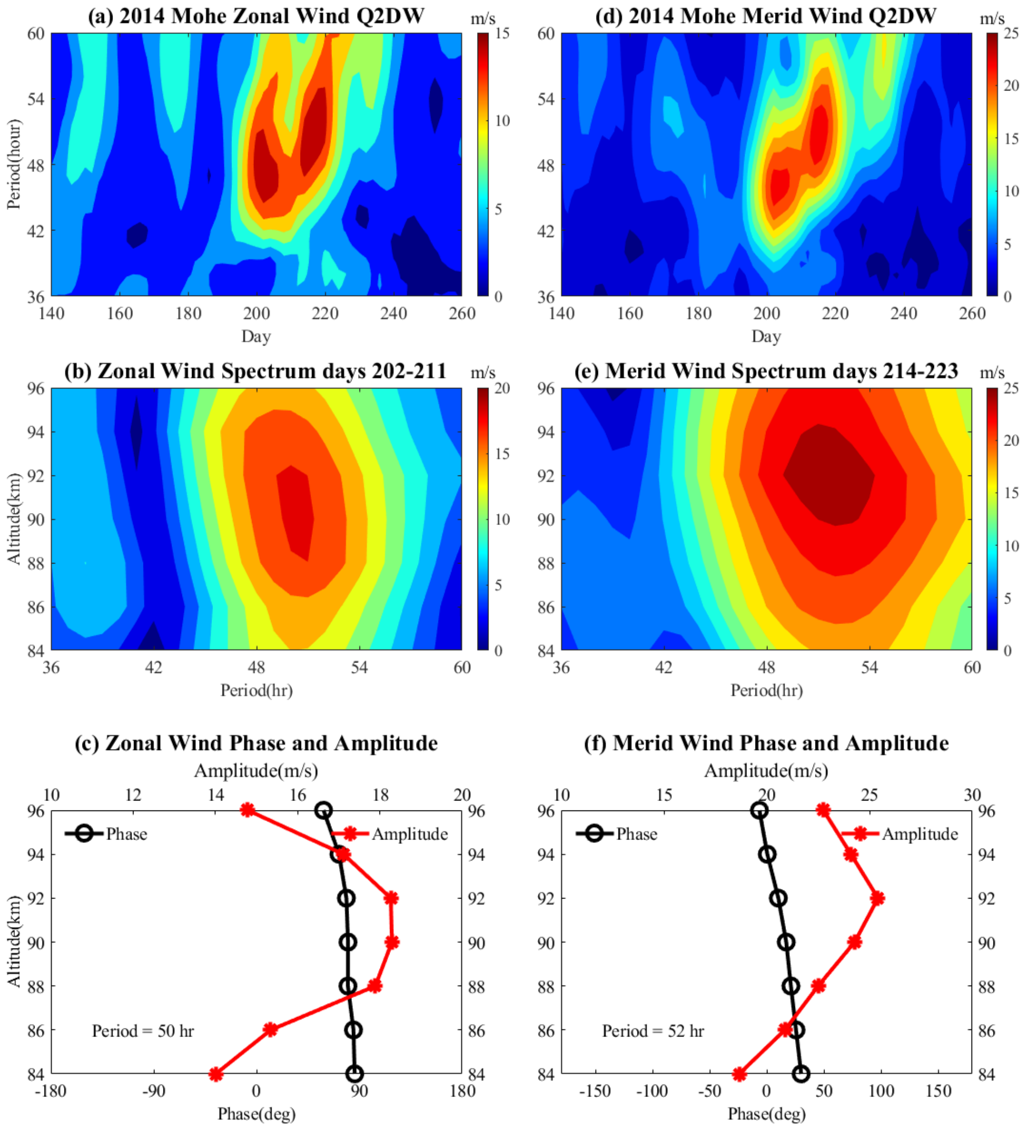

Figure 5. (**a**,**d**) Periodograms of the zonal and meridional amplitude for the years 2013–2022 at 90 km altitude. Each day represents the center of a 9-day analysis of wind data. (**b**,**e**) Zonal and horizontal wind spectra and the corresponding (**c**,**f**) Q2DW amplitudes and phases in days 202–211 (2014) and 214–223 (2014) for the zonal (**b**,**c**) and meridional (**e**,**f**) components. The phase of Q2DW is represented by the degree to which Q2DW reaches its maximum. The zonal and meridional components reach their maxima at approximately 50 and 52 h.

To further investigate the Q2DW variability in the Mohe winds, we recorded Q2DW events from 2013 to 2022 and performed a detailed analysis. A histogram plot of the Q2DW data for the Mohe wave is shown in Figure 6. Figure 6a shows a total of 65 zonal Q2DW events during the 2013–2022 summer seasons. Q2DWs occurred more frequently (27 times) on days 180–220 but less frequently on days 220–240 (3 times) and 140–160 (10 times). A total of 14 Q2DW events were recorded between days 180 and 220, accounting for 21.5% of the total. As shown in Figure 6c, the average amplitude of Q2DWs during days 200–220 is ~11 m/s, with minimum values occurring during days 240–260 (~5 m/s) and 160–180 (~6 m/s). From Figure 6b, it can be observed that the wave period of Q2DW is distributed in the range of ~36–60 h and the frequency of occurrence is 15 times larger in the range of ~51–54 h. This accounts for 23% of the total number of events, peaking in a period between ~45 and 54 h (36 times). Q2DW long-wave period events are distributed between ~54 and 60 h (nine times). As shown in Figure 6d, the average amplitude of the ~36–60 h Q2DW wave period is greater than ~6 m/s and the maximum amplitude occurs at ~39–45 h, ~48–51 h, and ~54–57 h (greater than ~8 m/s).

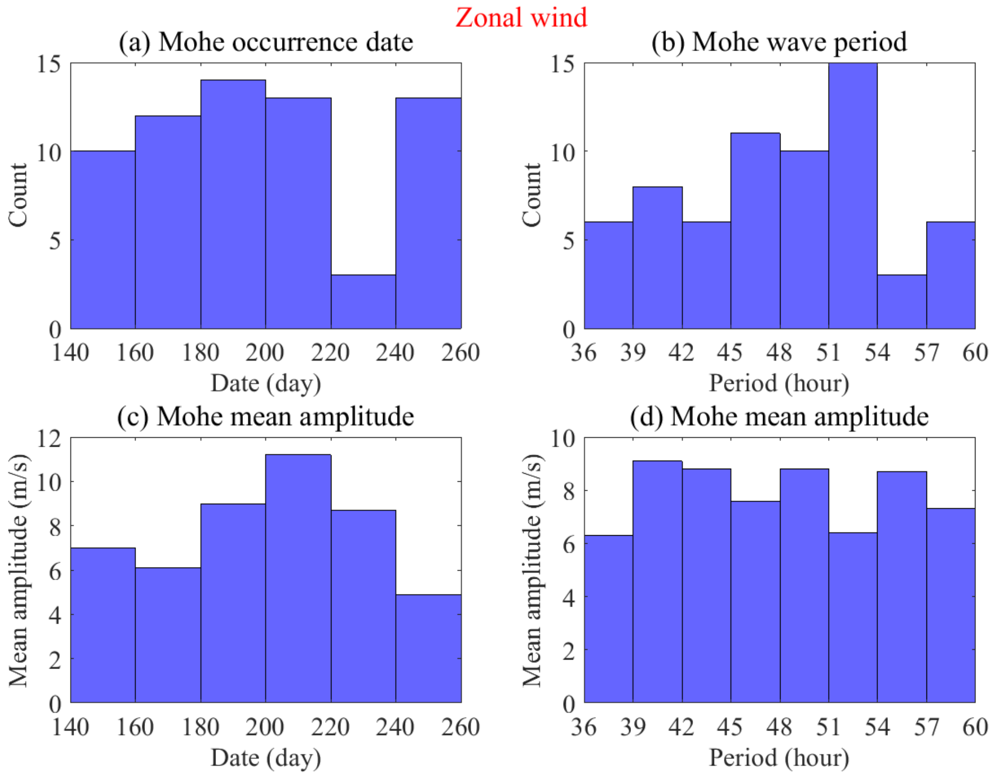

Figure 6. Statistical results for the boreal summer zonal wind Q2DW event at Mohe during 2013–2022. The occurrence dates and mean amplitudes of dates are shown in the left panel. The wave periods and mean amplitudes of periods are shown in the right panel.

Figure 7a shows 65 meridional Q2DW events from the 2013–2022 summer seasons. Q2DWs occurred more frequently (16 times) on days 180–200 but less frequently on days 220–240 (5 times), 140–160 (10 times), and 160–180 (10 times). A total of 29 Q2DW events were recorded between days 180 and 220, accounting for 44.6% of the total number of events. As shown in Figure 7c, the average amplitude of Q2DWs during days 220–240 is ~19 m/s, with minimum values occurring during days 240–260 (~5 m/s) and 140–160 (~7 m/s). From Figure 7b, it can be observed that the wave period of the Q2DWs is distributed in the range of ~36–60 h and the frequency of occurrence is 12 times in the range of ~45–48 h, accounting for 18.4% of the total number of events and culminating at between ~42 and 54 h (43 times). The long-wave period events of the Q2DWs are distributed between ~57 and 60 h (five times). As shown in Figure 7d, the average amplitude of the Q2DW wave period is greater than ~9 m/s and the maximum amplitude occurs at ~36–39 h and 48–51 h (~13 m/s).

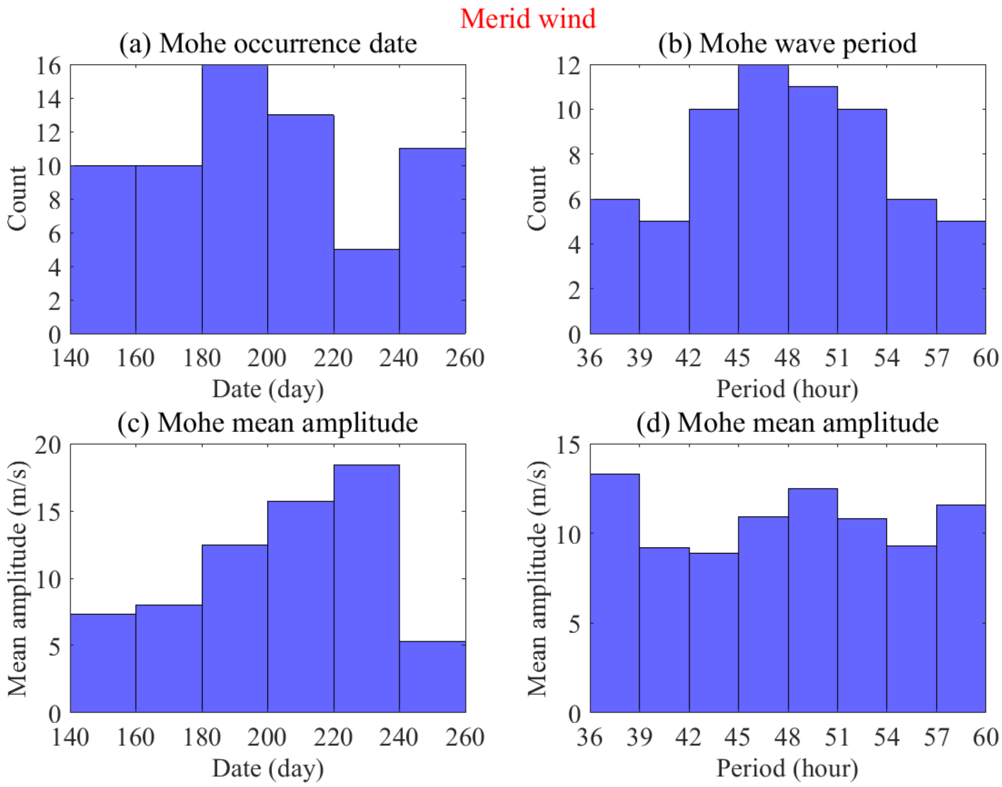

Figure 7. Same as Figure 6, but representing meridional wind.

3.3. Wuhan Q2DW

Similar to Figure 5, Figure 8 shows the mean period–date spectra of Wuhan zonal and meridional 90 km Q2DWs during the 2014 summer. At ~50 h during days 200–209, the zonal Q2DW reaches its summer maximum with an amplitude of ~20 m/s, as shown in Figure 8a. As can be seen in Figure 8b, the maximum amplitude of the zonal Q2DW at ~90 km has a period of ~50 h and reaches an amplitude of ~25 m/s, which further confirms the validity of this Q2DW event. Figure 8e shows the meridional Q2DW amplitude, which peaks at ~90 km at ~50 h and reaches a maximum of ~35 m/s. The phase and amplitude of the Q2DW events are shown in Figure 8c,f, with the phase slope calculated as the vertical wavelength of the Q2DW. As shown in Figure 8c, the vertical wavelength of the ~50 h zonal Q2DW is estimated to be ~110 km, while the vertical wavelength of the ~50 h meridional Q2DW is estimated to be ~50 km (Figure 8f).

The zonal Q2DW information for Wuhan is shown as a histogram diagram in Figure 9. Figure 9a shows that zonal Q2DW events occurred 77 times during the 2013–2022 summer seasons. The frequency of Q2DWs was higher during days 240–260 (17 times) and lower during days 160–180 (10 times). A significant portion (32 in total) of these events was recorded between days 220 and 240, constituting 41.5% of total occurrences. As shown in Figure 9c, the average amplitude of the Q2DW during days 200–220 is ~12 m/s, with a minimum amplitude of ~9 m/s during the summer. From Figure 9b, it can be seen that the wave period of the Q2DW is distributed over a range of ~36–60 h. In the range of ~36–39 h, it peaks on 17 occurrences and accounts for 22% of the total number of events, followed by 15 events in the range of ~48–51 h. Q2DW long-wave period events are distributed between ~57 and 60 h (seven times). As shown in Figure 9d, the average amplitude of the Q2DWs is larger than ~8 m/s at ~36–60 h, and the maximum occurs at ~51–54 and ~54–57 h, reaching ~13 m/s and ~12 m/s.

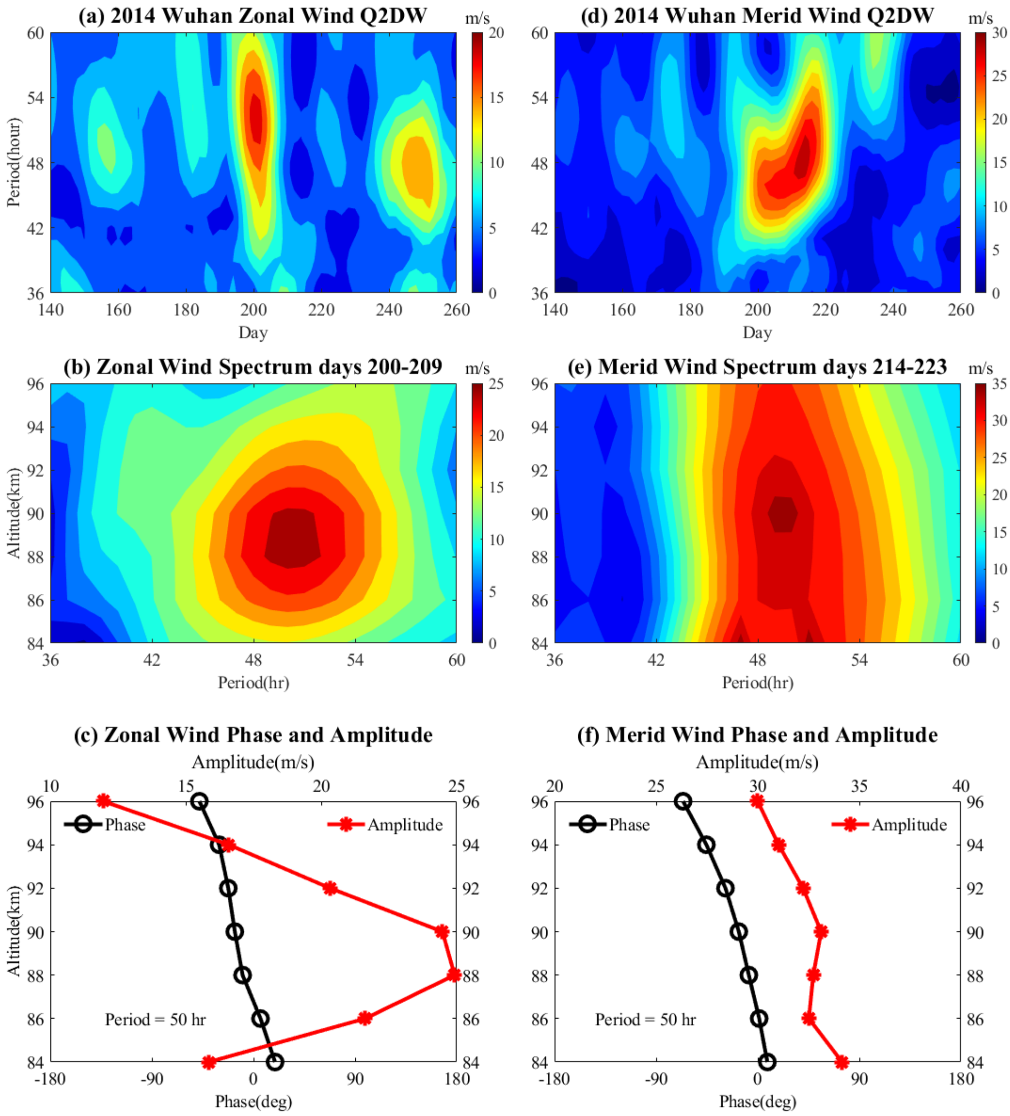

Figure 8. Same as Figure 5, but representing Wuhan. Both the meridional and zonal components maximize at ~50 h.

Similarly, we statistically analyzed the characteristics of the Wuhan meridional Q2DWs. The histogram plot of the Wuhan Q2DW data in Figure 10a shows a total of 76 meridional Q2DW events in the summers of 2013–2022. Q2DWs more frequently occurred (19 times) during days 220–240, accounting for 25% of the total. Q2DWs occurred five times during days 220–240 and ten times during days 180–200, with less frequency. As shown in Figure 10c, the average amplitude of Q2DWs during days 180 to 220 is ~20 m/s, with the minimum appearing during days 240 to 260 (~8 m/s). As can be seen in Figure 10b, the wave period of the Q2DW is spread over a range of ~36–60 h, and the frequency of occurrence is 17 times larger over a range of ~48–51 h. It accounted for 22.4% of the total number of events, peaking between 45 and 51 h (31 times). The long-wave period events of the Q2DW are distributed between ~57 and 60 h (seven times). As shown in Figure 10d, the average minimum amplitude of Q2DW at ~54–57 h is ~9 m/s, and the maximum amplitude is at ~42–45 h (18 m/s).

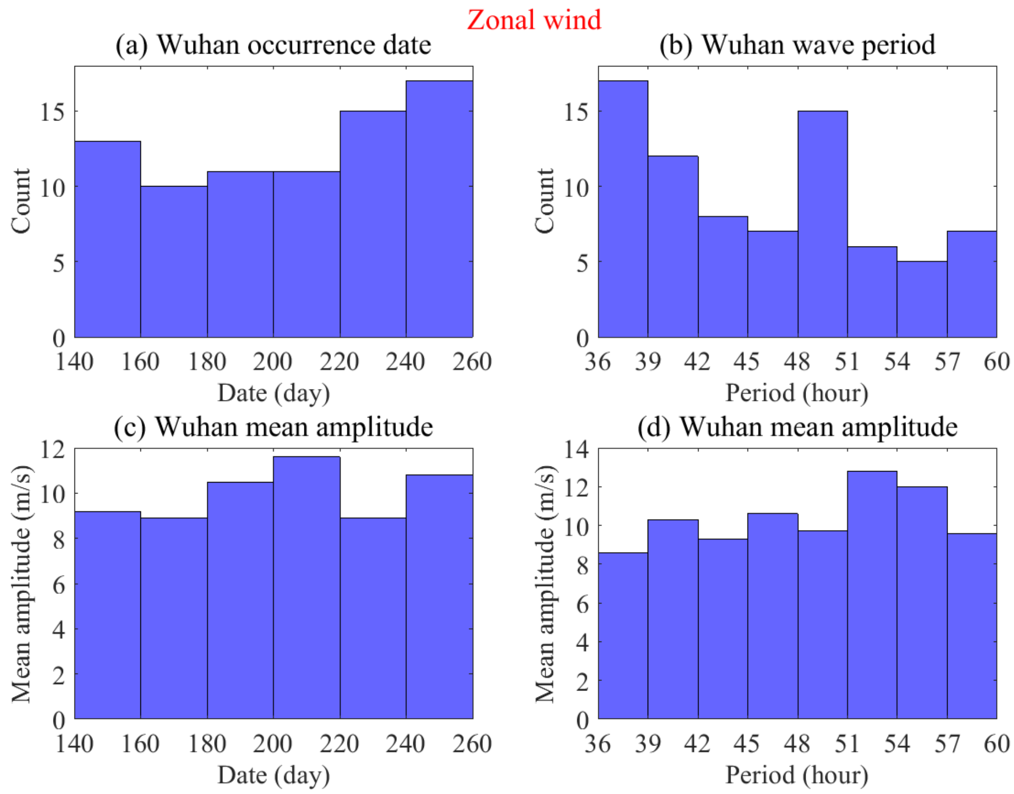

Figure 9. Same as Figure 6, but representing Wuhan.

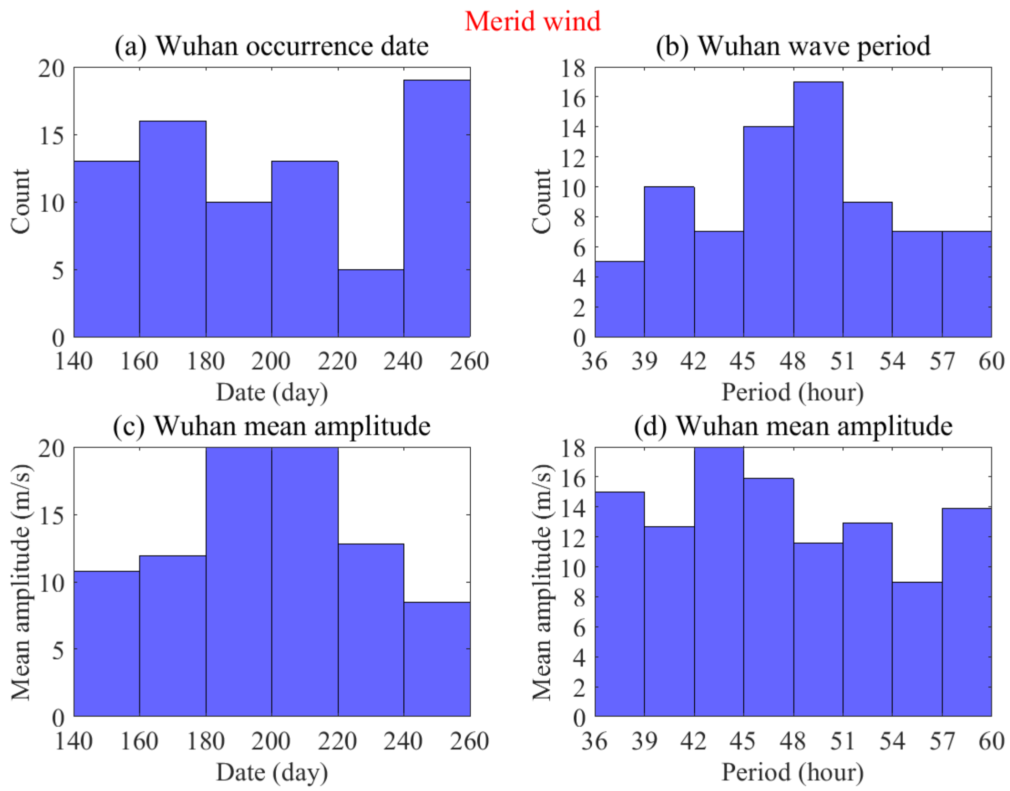

Figure 10. Same as Figure 9, but representing meridional wind.

To further investigate the amplitude and period variability in the Mohe and Wuhan Q2DWs during the 2013–2022 summer seasons, we summarize the maximum amplitudes of the zonal and meridional Q2DWs for each year and their corresponding wave periods and occurrence dates.

The Mohe zonal and meridional Q2DW events are most frequently observed during days 200–220 (five times), slightly less frequently during days 180–200 (four times), and only once during days 220–240, as shown in Figure 11a. The strongest Wuhan zonal and meridional Q2DWs are amplified four times during days 200–220, three times during days 180–220 for meridional Q2DWs, and two times during days 180–220 for zonal Q2DWs (Figure 11b). From Figure 11c, it can be observed that five Mohe zonal Q2DW events with wave periods of ~51–54 h are present, and short-period events occur twice between ~42 and 45 h. In addition, the wave periods of the four meridional Q2DW events are distributed over ~48–51 h, and the long-period events occur between ~54 and 60 h in two cases. The three Wuhan zonal and meridional Q2DW events have wave periods within ~48–51 and ~51–54 h, respectively, accounting for 30% of the total, with event periods between ~45 and 57 h being more abundant than those with adjacent periods. Only one zonal Q2DW event with wave periods of ~36–39 h and ~57–60 h is recognized, as shown in Figure 11d. The amplitudes of the Mohe zonal Q2DWs could reach as large as ~8–12 m/s, which occurs five times; ~12–16 m/s slightly less frequently (three times); and ~16–20 m/s, ~20–24 m/s, and ~28–32 m/s only once (Figure 11e). The amplitudes of the meridional Q2DWs could reach as large as ~12–20 m/s, which occurs eight times; ~28–32 m/s slightly less frequently (two times); and ~24–28 m/s only once. The Wuhan amplitudes of the 10 zonal Q2DW events are distributed within ~10–20 m/s. In addition, the amplitudes of the meridional Q2DWs could reach as large as ~20–30 m/s, which occurs five times; ~10–20 m/s slightly less frequently (three times); and ~30–40 m/s and ~40–50 m/s only once, respectively (Figure 11f). We identified a significant difference in the behavior of the Q2DWs at high and middle latitudes. The Q2DW occurrence dates at higher latitudes are more concentrated, while those at middle latitudes are different. In the distribution of wave periods, the Q2DWs at high and middle latitudes are significantly different, with high-latitude waves exhibiting longer periods than middle-latitude Q2DWs. The opposite is true at mid-latitudes. In terms of amplitude variability, the Q2DW amplitude is significantly stronger at middle latitudes than at high latitudes.

Shown in Figure 12a,b are the vertical profiles of the amplitude and phase of the Mohe Q2DWs in zonal and meridional winds. The amplitude of the Q2DW is maximized at ~88 km for both zonal and meridional winds. The zonal and meridional winds show estimated vertical wavelengths of ~144 km and ~200 km, both for ~45 h Q2DWs. Figure 12c,d show the annual mean zonal and meridional wind speeds at Mohe for days 140–260 between 2013 and 2022. The data within the black dashed line are the primary occurrence dates of the Q2DWs, and the phase and amplitude of the Q2DWs are analyzed using these data. Figure 12e,f show the vertical profiles of the amplitude and phase of the Wuhan Q2DWs in zonal and meridional winds. The maximum amplitudes of the Q2DWs for zonal and meridional winds are observed at ~88 km and ~90 km. The vertical wavelength of the zonal wind for the ~56 h Q2DW is estimated to be ~36 km. The vertical wavelength of the meridional wind for the ~50 h Q2DW is estimated to be ~33 km. Figure 12g,h are similar to Figure 12c,d but for the Wuhan data. We identified that the phases of the Q2DWs are significantly different at high and middle latitudes. Higher latitude Q2DWs have longer vertical wavelengths, while mid-latitude Q2DWs have shorter vertical wavelengths. Annual mean zonal and meridional winds are also different, with winds stronger at mid-latitudes than at higher latitudes.

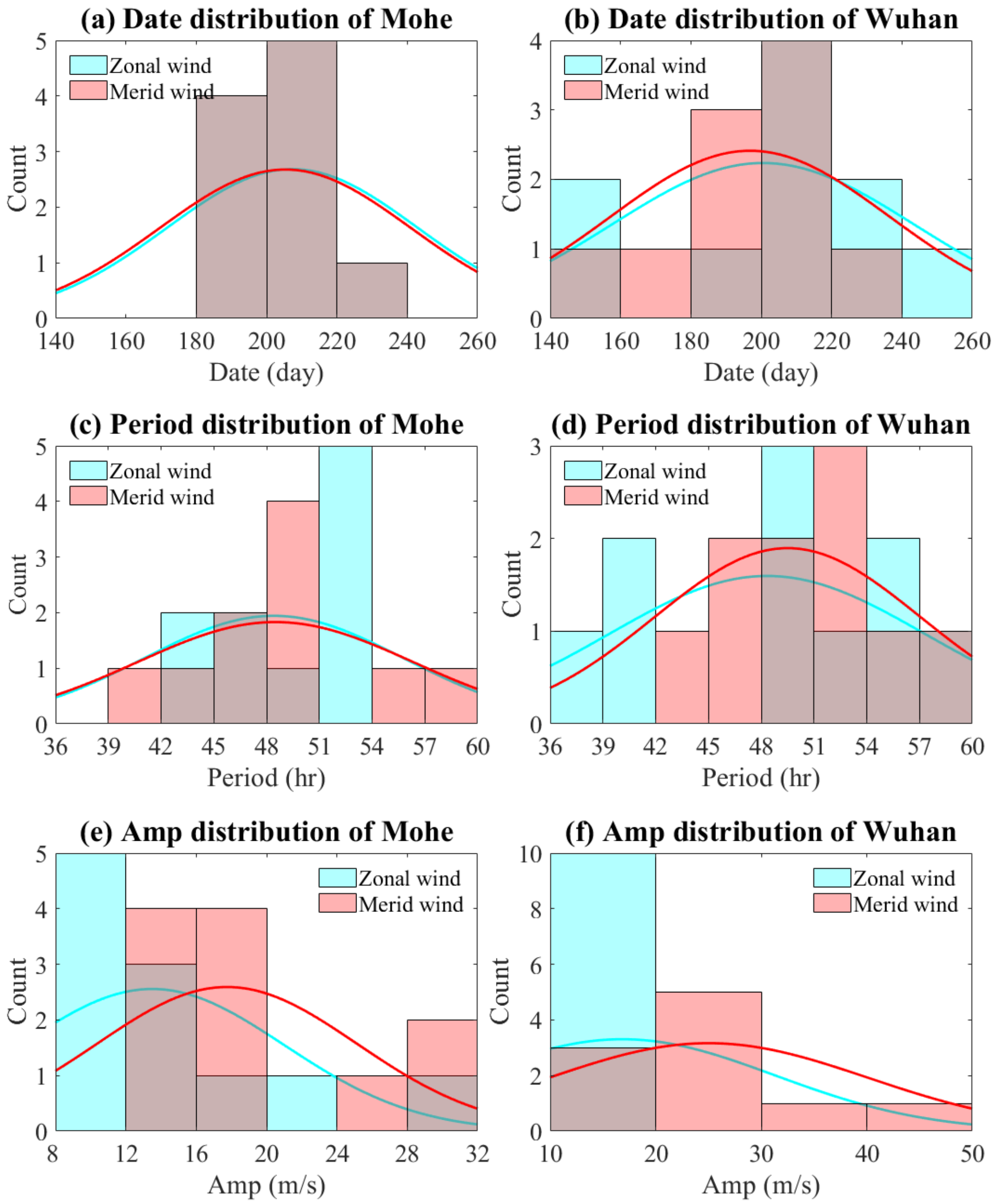

Figure 11. Statistical results for the occurrence dates (**a**,**b**), periods (**c**,**d**), and amplitude of dates (**e**,**f**) for Mohe and Wuhan. The approximate curve is fitted by a normal distribution with a confidence interval of 0.95.

Figure 13 shows the amplitude and period of the meridional Q2DWs in the Mohe and Wuhan zones during the 2013–2022 summer seasons. The observed amplitudes of the Mohe zonal Q2DWs are as large as ~13–23 m/s in 2014, 2017, 2019, and 2021, with an amplitude of ~23 m/s in 2017. The strongest Wuhan zonal Q2DWs are observed in 2014, 2018, 2019, 2020, and 2022, with an amplitude of ~15–19 m/s. During 2013, 2014, 2016, 2017, 2019, 2020, 2021, and 2022, the maximum amplitudes of the Mohe meridional Q2DWs are also equal to or larger than ~13 m/s. The amplitudes of the Wuhan meridional Q2DWs during 2013, 2014, 2017, 2019, 2020, 2021, and 2022 also reach ~20–44 m/s. The wave period of the Mohe zonal Q2DWs during the summer is the most robust during 2014, 2015, 2016, 2018, 2020, and 2022 at ~50–53 h, which is slightly smaller than that for ~42–45 h during 2017, 2019, and 2021. The wave periods of the Wuhan zonal Q2DWs were observed in 2014, 2017, 2021, and 2022 at ~52–59 h. In addition, the shorter wave periods in 2013, 2019, and 2020 reached ~38–40 h. The Mohe meridional Q2DWs had the longest wave periods during

2019 and 2020 at ~56–57 h. In addition, the shorter wave periods in 2021 and 2022 reached ~41–43 h. The wave periods of the Wuhan meridional Q2DWs during 2013, 2018, 2019, and 2021 only reached ~51–58 h, and shorter wave periods of ~44–45 h are observed during 2017 and 2020. In addition, the 2017 Mohe zonal and meridional Q2DWs are specific, and their amplitudes are unusually strong. The variability in solar activity during 2013–2016 is similar to the trend of zonal and meridional amplitude and wave periods, but it differs in 2018–2020. Similarly, the correlation between the wave period change trend in Wuhan and the change in solar activity is also low.

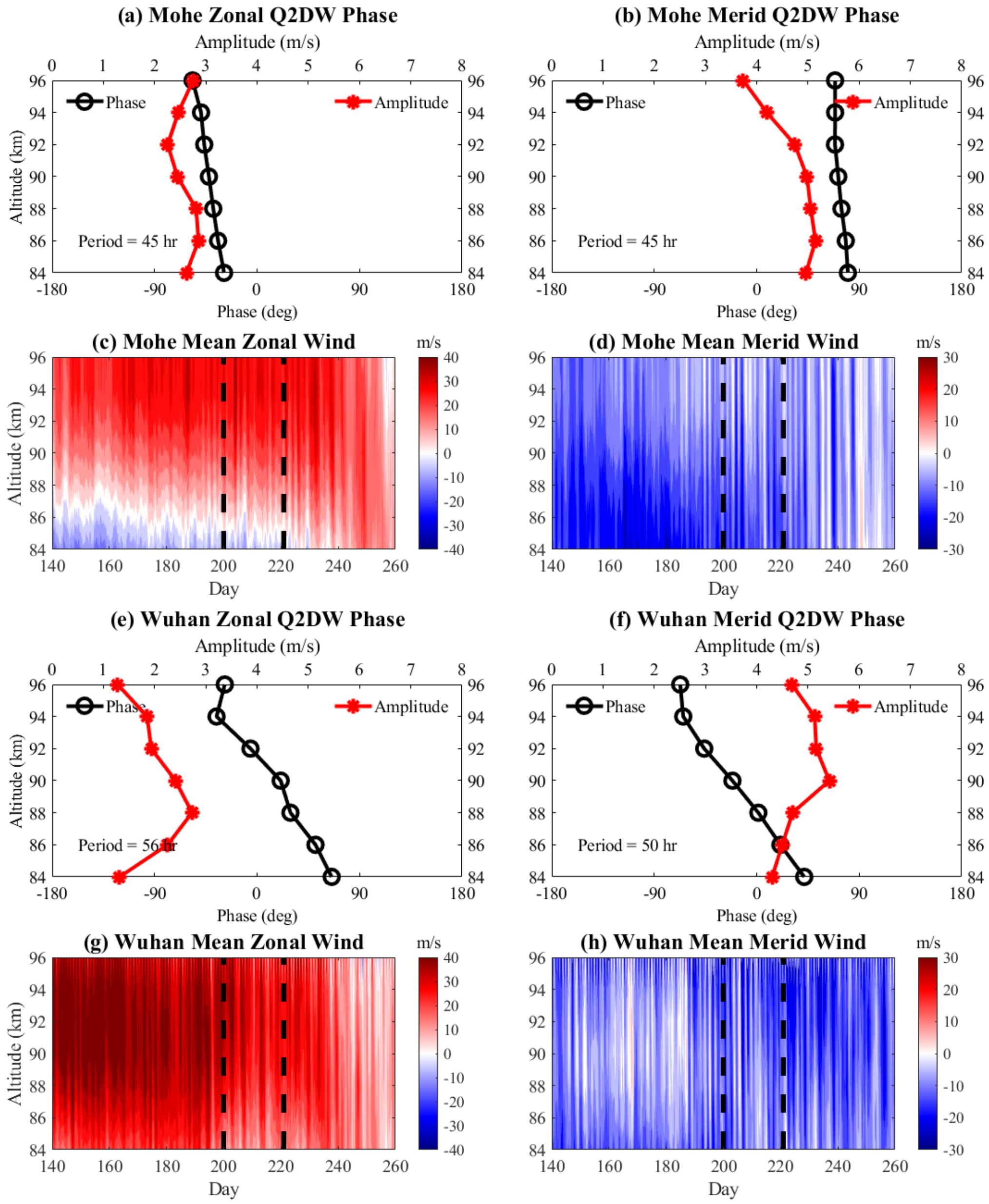

Figure 12. Mean Q2DW amplitudes and phases in days 200–220 during 2013–2022 for the zonal (**a**,**e**) and meridional (**b**,**f**) components. Mean zonal and meridional winds observed from the meteor radar at Mohe (**c**,**d**) and Wuhan (**g**,**h**) during 2013–2022. The black dashed line represents the selected 200–220 day zonal and meridional wind data.

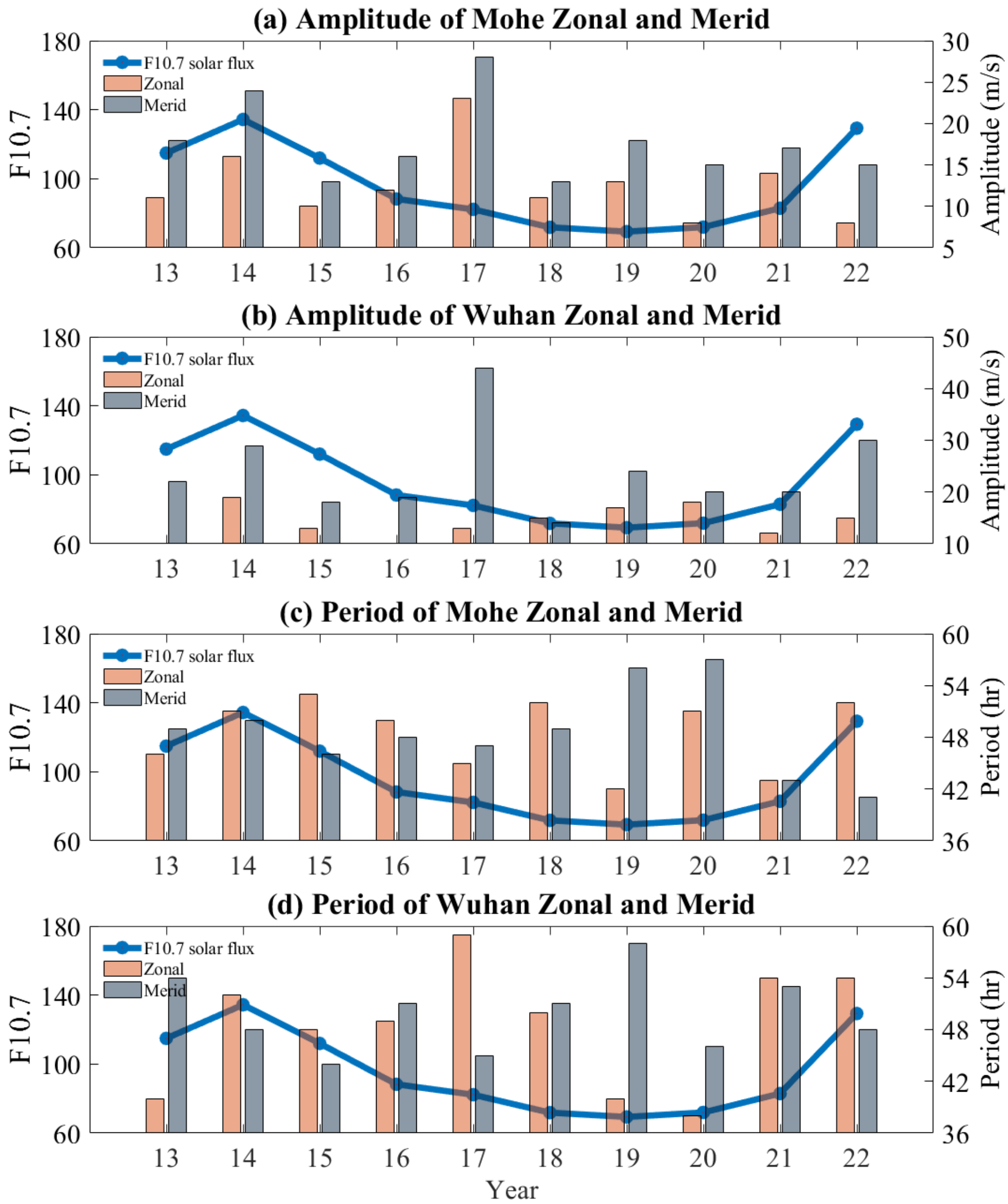

Figure 13. The strongest zonal and meridional amplitudes during the 2013–2022 boreal summer periods for Mohe and Wuhan (**a**,**b**). The blue line represents the boreal summer mean (10.7 cm) solar flux. The orange and gray bars represent the zonal and meridional Q2DWs. (**c**,**d**) are the periods corresponding to (**a**,**b**). (**c**,**d**) are periods corresponding to (**a**,**b**).

4. Discussion

We find that the occurrence dates of zonal and meridional Q2DWs in high-latitude Mohe are consistent, with all being concentrated during days 180–240 and most prominent during days 200–220, which is consistent with the findings of Pancheva [44] obtained using satellite data. Similarly, there are differences in the occurrence dates of zonal and meridional Q2DWs in mid-latitude Wuhan. According to the normal curves, zonal Q2DWs tend to occur in late summer, while meridional Q2DWs tend to occur in early summer, but they also occur most frequently during days 200–220. We can observe that there is a difference between the wave periods of the zonal and meridional Q2DWs in high-latitude Mohe. This is related to the selective amplification of Q2DWs via the background atmosphere [45]. Zonal Q2DWs are more concentrated at ~51–54 h, while meridional Q2DWs are more concentrated at ~48–51 h, indicating that zonal Q2DWs have a longer period than meridional Q2DWs. Similarly, the zonal and meridional Q2DW periods in mid-latitude Wuhan are also different, but unlike Mohe, the zonal Q2DW period in Wuhan is concentrated at ~48–51 h, being shorter than the meridional Q2DW period of ~51–54 h, which is consistent with the findings of Lilienthal [2]. The zonal and meridional Q2DW amplitudes are significantly different for high-latitude Mohe, with the meridional Q2DW amplitude (~30 m/s) being larger than the zonal one (~10 m/s). The same feature is observed for mid-latitude Wuhan, where the meridional Q2DW amplitude (~45 m/s) is much larger than the zonal one (~15 m/s). It can be seen that there is a difference between the high- and mid-latitude Q2DWs. The Q2DW occurrence dates are concentrated at high latitudes, while at middle latitudes, zonal and meridional Q2DWs tend to occur in late and early summer, respectively. Zonal Q2DWs have a longer period at high latitudes compared to meridional Q2DWs, while meridional Q2DWs have a longer period at middle latitudes compared to zonal ones. Zonal Q2DW amplitudes are weaker than meridional Q2DW amplitudes at high and middle latitudes. These observations, combined with the fact that Gu [6] and Lilienthal [2] report a strong summer Q2DW at high and middle latitudes, indicate that the influence of summer Q2DWs becomes stronger with descending latitudes.

The vertical wavelengths of high-latitude zonal and meridional Q2DWs over Mohe are longer than those at middle latitudes, and the speeds of the zonal and meridional winds at middle latitudes are stronger than those at high latitudes, indicating that the stronger background wind at middle latitudes can provide sufficient energy for the propagation and amplification of Q2DWs. As wind shear is a proxy for baroclinic instability, we conclude that Q2DWs over Mohe and Wuhan are forced, at least in part, via the summer instability of the mesosphere jet, which is consistent with the findings of Lilienthal [2]. Gu [46] observed increasing Q2DW amplitudes above regions of negative quasi-geostrophic potential vorticity using satellite measurements. At high and mid-latitudes, the amplitudes and wave period sof Q2DWs in the calendar year do not show a strong correlation with F10.7 solar activity, but there is a similar trend across some years.

5. Summary

We present the first extensive study of zonal and meridional Q2DW activity in the MLT region during the 2013–2022 summer seasons, using the wind datasets from the Mohe and Wuhan meteorological radars. We calculated the Q2DW events in Mohe and Wuhan at ~90 km in both zonal and meridional winds. The amplitude and wave period for each event is determined via least-squares fitting. Our study covers the interannual variability in Q2DWs at high and middle latitudes between 2013 and 2022 and analyzes the differences in the behavior of Q2DWs at high and middle latitudes.

Overall, we have studied the interannual variability in zonal and meridional Q2DWs at the high and mid-latitudes of the MLT region. Additionally, we statistically analyzed the differences in the behavioral variability in the peak amplitude, wave period, and occurrence date of Q2DWs between Mohe and Wuhan in the MLT region.

Author Contributions: Conceptualization, L.T. and S.-Y.G.; software, L.T.; validation, L.T., S.-Y.G. and X.D.; formal analysis, L.T.; investigation, L.T.; resources, S.-Y.G. and X.D.; writing—original draft preparation, L.T.; writing—review and editing, L.T., S.-Y.G., R.S. and X.D.; funding acquisition, S.-Y.G. and X.D. All authors have read and agreed to the published version of the manuscript.

Funding: This work was funded by the National Natural Science Foundation of China (41831071, 42188101).

Institutional Review Board Statement: Not applicable.

Informed Consent Statement: Not applicable.

Data Availability Statement: The Mohe and Wuhan meteor radar data are available from https://www.nssdc.ac.cn, accessed on 1 November 2023.

Acknowledgments: We acknowledge for the data resources from the "National Space Science Data Center, National Science & Technology Infrastructure of China. (https://www.nssdc.ac.cn, accessed on 1 November 2023)".

Conflicts of Interest: The authors declare no conflict of interest.

References

1. Pancheva, D.; Mukhtarov, P.; Siskind, D.E. Climatology of the quasi-2-day waves observed in the MLS/Aura measurements (2005–2014). *J. Atmos. Sol. Terr. Phys.* **2018**, *171*, 210–224. [CrossRef]
2. Lilienthal, F.; Jacobi, C. Meteor radar quasi 2-day wave observations over 10 years at Collm (51.3°N, 13.0°E). *Atmos. Chem. Phys.* **2015**, *15*, 9917–9927. [CrossRef]
3. Gu, S.-Y.; Tang, L.; Hou, X.; Zhao, H.; Teng, C.-K.-M.; Dou, X. Quasi-Two-Day Waves in the Northern Hemisphere Observed by TIMED/SABER Measurements during 2002–2019. *J. Geophys. Res. Space Phys.* **2021**, *126*, e2020JA028877. [CrossRef]
4. Liu, G.; England, S.L.; Janches, D. Quasi Two-, Three-, and Six-Day Planetary-Scale Wave Oscillations in the Upper Atmosphere Observed by TIMED/SABER over ~17 Years during 2002–2018. *J. Geophys. Res. Space Phys.* **2019**, *124*, 9462–9474. [CrossRef]
5. Lainer, M.; Hocke, K.; Kämpfer, N. Long-term observation of midlatitude quasi 2-day waves by a water vapor radiometer. *Atmos. Chem. Phys.* **2018**, *18*, 12061–12074. [CrossRef]
6. Gu, S.-Y.; Li, T.; Dou, X.; Wang, N.-N.; Riggin, D.; Fritts, D. Long-term observations of the quasi two-day wave by Hawaii MF radar. *J. Geophys. Res. Space Phys.* **2013**, *118*, 7886–7894. [CrossRef]
7. Tunbridge, V.M.; Sandford, D.J.; Mitchell, N.J. Zonal wave numbers of the summertime 2 day planetary wave observed in the mesosphere by EOS Aura Microwave Limb Sounder. *J. Geophys. Res. Atmos.* **2011**, *116*, D11103. [CrossRef]
8. Suresh Babu, V.; Kishore Kumar, K.; John, S.R.; Subrahmanyam, K.V.; Ramkumar, G. Meteor radar observations of short-term variability of quasi 2 day waves and their interaction with tides and planetary waves in the mesosphere–lower thermosphere region over Thumba (8.5°N, 77°E). *J. Geophys. Res. Atmos.* **2011**, *116*, D16121. [CrossRef]
9. Wu, D.L.; Fishbein, E.F.; Read, W.G.; Waters, J.W. Excitation and Evolution of the Quasi-2-Day Wave Observed in UARS/MLS Temperature Measurements. *J. Atmos. Sci.* **1996**, *53*, 728–738. [CrossRef]
10. Meek, C.E.; Manson, A.H.; Franke, S.J.; Singer, W.; Hoffmann, P.; Clark, R.R.; Tsuda, T.; Nakamura, T.; Tsutsumi, M.; Hagan, M.; et al. Global study of northern hemisphere quasi-2-day wave events in recent summers near 90 km altitude. *J. Atmos. Terr. Phys.* **1996**, *58*, 1401–1411. [CrossRef]
11. Tang, L.; Gu, S.Y.; Dou, X.K. Eastward-propagating planetary waves in the polar middle atmosphere. *Atmos. Chem. Phys.* **2021**, *21*, 17495–17512. [CrossRef]
12. Yamazaki, Y.; Stolle, C.; Matzka, J.; Alken, P. Quasi-6-Day Wave Modulation of the Equatorial Electrojet. *J. Geophys. Res. Space Phys.* **2018**, *123*, 4094–4109. [CrossRef]
13. Forbes, J.M.; Zhang, X. The quasi-6 day wave and its interactions with solar tides. *J. Geophys. Res. Space Phys.* **2017**, *122*, 4764–4776. [CrossRef]
14. Pancheva, D.; Mukhtarov, P.; Andonov, B.; Forbes, J.M. Global distribution and climatological features of the 5–6-day planetary waves seen in the SABER/TIMED temperatures (2002–2007). *J. Atmos. Sol. Terr. Phys.* **2010**, *72*, 26–37. [CrossRef]
15. Riggin, D.M.; Fritts, D.C.; Tsuda, T.; Nakamura, T.; Vincent, R.A. Radar observations of a 3-day Kelvin wave in the equatorial mesosphere. *J. Geophys. Res. Atmos.* **1997**, *102*, 26141–26157. [CrossRef]
16. Allen, D.R.; Stanford, J.L.; Elson, L.S.; Fishbein, E.F.; Froidevaux, L.; Waters, J.W. The 4-Day Wave as Observed from the Upper Atmosphere Research Satellite Microwave Limb Sounder. *J. Atmos. Sci.* **1997**, *54*, 420–434. [CrossRef]
17. Lawrence, B.N.; Fraser, G.J.; Vincent, R.A.; Phillips, A. The 4-Day Wave in the Antarctic Mesosphere. *J. Geophys. Res.-Atmos.* **1995**, *100*, 18899–18908. [CrossRef]
18. Randel, W.J.; Lait, L.R. Dynamics of the 4-Day Wave in the Southern Hemisphere Polar Stratosphere. *J. Atmos. Sci.* **1991**, *48*, 2496–2508. [CrossRef]
19. Yamazaki, Y.; Matthias, V. Large-Amplitude Quasi-10-Day Waves in the Middle Atmosphere during Final Warmings. *J. Geophys. Res. Atmos.* **2019**, *124*, 9874–9892. [CrossRef]
20. Forbes, J.M.; Zhang, X. Quasi-10-day wave in the atmosphere. *J. Geophys. Res. Atmos.* **2015**, *120*, 11079–11089. [CrossRef]
21. Liu, J.; Zhang, D.; Hao, Y.; Xiao, Z. Multi-instrumental Observations of the Quasi-16-Day Variations from the Lower Thermosphere to the Topside Ionosphere in the Low-Latitude Eastern Asian Sector During the 2017 Sudden Stratospheric Warming Event. *J. Geophys. Res. Space Phys.* **2020**, *125*, e2019JA027505. [CrossRef]
22. Gong, Y.; Ma, Z.; Li, C.; Lv, X.; Zhang, S.; Zhou, Q.; Huang, C.; Huang, K.; Yu, Y.; Li, G. Characteristics of the quasi-16-day wave in the mesosphere and lower thermosphere region as revealed by meteor radar, Aura satellite, and MERRA2 reanalysis data from 2008 to 2017. *Earth Planet. Phys.* **2020**, *4*, 274–284. [CrossRef]
23. Gong, Y.; Wang, H.; Ma, Z.; Zhang, S.; Zhou, Q.; Huang, C.; Huang, K. A Statistical Analysis of the Propagating Quasi 16-Day Waves at High Latitudes and Their Response to Sudden Stratospheric Warmings from 2005 to 2018. *J. Geophys. Res. Atmos.* **2019**, *124*, 12617–12630. [CrossRef]
24. Day, K.A.; Taylor, M.J.; Mitchell, N.J. Mean winds, temperatures and the 16- and 5-day planetary waves in the mesosphere and lower thermosphere over Bear Lake Observatory (42°N, 111°W). *Atmos. Chem. Phys.* **2012**, *12*, 1571–1585. [CrossRef]
25. Day, K.A.; Hibbins, R.E.; Mitchell, N.J. Aura MLS observations of the westward-propagating s = 1, 16-day planetary wave in the stratosphere, mesosphere and lower thermosphere. *Atmos. Chem. Phys.* **2011**, *11*, 4149–4161. [CrossRef]
26. Muller, H.G.; Massey, H.S.W.; Groves, G.V. A discussion on D and E region winds over Europe—Long-period meteor wind oscillations. *Math. Phys. Sci.* **1972**, *271*, 585–599. [CrossRef]

27. Watanabe, S.; Tomikawa, Y.; Sato, K.; Kawatani, Y.; Miyazaki, K.; Takahashi, M. Simulation of the eastward 4-day wave in the Antarctic winter mesosphere using a gravity wave resolving general circulation model. *J. Geophys. Res. Atmos.* **2009**, *114*, D16111. [CrossRef]
28. Manney, G.L.; Orsolini, Y.J.; Pumphrey, H.C.; Roche, A.E. The 4-Day Wave and Transport of UARS Tracers in the Austral Polar Vortex. *J. Atmos. Sci.* **1998**, *55*, 3456–3470. [CrossRef]
29. Fraser, G.J.; Hernandez, G.; Smith, R.W. Eastward-moving 2–4 day waves in the winter Antarctic mesosphere. *Geophys. Res. Lett.* **1993**, *20*, 1547–1550. [CrossRef]
30. Venne, D.E.; Stanford, J.L. Observation of a 4–Day Temperature Wave in the Polar Winter Stratosphere. *J. Atmos. Sci.* **1979**, *36*, 2016–2019. [CrossRef]
31. Jacobi, C.; Fröhlich, K.; Pogoreltsev, A. Quasi two-day-wave modulation of gravity wave flux and consequences for the planetary wave propagation in a simple circulation model. *J. Atmos. Sol. Terr. Phys.* **2006**, *68*, 283–292. [CrossRef]
32. Jacobi, C.; Portnyagin, Y.I.; Merzlyakov, E.G.; Kashcheyev, B.L.; Oleynikov, A.N.; Kürschner, D.; Mitchell, N.J.; Middleton, H.R.; Muller, H.G.; Comley, V.E. Mesosphere/lower thermosphere wind measurements over Europe in summer 1998. *J. Atmos. Sol. Terr. Phys.* **2001**, *63*, 1017–1031. [CrossRef]
33. Ma, Z.; Gong, Y.; Zhang, S.; Zhou, Q.; Huang, C.; Huang, K.; Yu, Y.; Li, G.; Ning, B.; Li, C. Responses of Quasi 2 Day Waves in the MLT Region to the 2013 SSW Revealed by a Meteor Radar Chain. *Geophys. Res. Lett.* **2017**, *44*, 9142–9150. [CrossRef]
34. Holdsworth, D.A.; Reid, I.M.; Cervera, M.A. Buckland Park all-sky interferometric meteor radar. *Radio Sci.* **2004**, *39*, RS5009. [CrossRef]
35. Hall, C.M.; Aso, T.; Tsutsumi, M. An examination of high latitude upper mesosphere dynamic stability using the Nippon/Norway Svalbard Meteor Radar. *Geophys. Res. Lett.* **2002**, *29*, 121-1–121-3. [CrossRef]
36. Stober, G.; Jacobi, C.; Fröhlich, K.; Oberheide, J. Meteor radar temperatures over Collm (51.3°N, 13°E). *Adv. Space Res.* **2008**, *42*, 1253–1258. [CrossRef]
37. Hall, C.M.; Aso, T.; Tsutsumi, M.; Hffner, J.; Sigernes, F.; Holdsworth, D.A. Neutral air temperatures at 90 km and 70°N and 78°N. *J. Geophys. Res.Atmos.* **2006**, *111*, D14105. [CrossRef]
38. Hocking, W.K.; Fuller, B.; Vandepeer, B. Real-time determination of meteor-related parameters utilizing modern digital technology. *J. Atmos. Sol. Terr. Phys.* **2001**, *63*, 155–169. [CrossRef]
39. Yi, W.; Reid, I.M.; Xue, X.; Murphy, D.J.; Hall, C.M.; Tsutsumi, M.; Ning, B.; Li, G.; Younger, J.P.; Chen, T.; et al. High- and Middle-Latitude Neutral Mesospheric Density Response to Geomagnetic Storms. *Geophys. Res. Lett.* **2018**, *45*, 436–444. [CrossRef]
40. Liu, L.; Liu, H.; Chen, Y.; Le, H.; Sun, Y.-Y.; Ning, B.; Hu, L.; Wan, W. Variations of the meteor echo heights at Beijing and Mohe, China. *J. Geophys. Res. Space Phys.* **2017**, *122*, 1117–1127. [CrossRef]
41. Yu, Y.; Wan, W.; Ning, B.; Liu, L.; Wang, Z.; Hu, L.; Ren, Z. Tidal wind mapping from observations of a meteor radar chain in December 2011. *J. Geophys. Res. Space Phys.* **2013**, *118*, 2321–2332. [CrossRef]
42. Xiong, J.G.; Wan, W.; Ning, B.; Liu, L. First results of the tidal structure in the MLT revealed by Wuhan Meteor Radar (30°40′N, 114°30′E). *J. Atmos. Sol. Terr. Phys.* **2004**, *66*, 675–682. [CrossRef]
43. Sun, R.D.; Gu, S.Y.; Dou, X.K.; Wei, Y.F.; Qin, Y.S.; Yang, Z.L. Decadal Quasi-2-Day Wave Observations in the Equatorial Mesopause Region by a Meteor Radar over Kototabang (0.2°S, 100.3°E) and TIMED/TIDI and Comparison with Quasi-2-Day Wave Observations at Mid-Latitudes. *Remote Sens.* **2023**, *15*, 1122. [CrossRef]
44. Pancheva, D.; Mukhtarov, P.; Siskind, D.E.; Smith, A.K. Global distribution and variability of quasi 2 day waves based on the NOGAPS-ALPHA reanalysis model. *J. Geophys. Res. Space Phys.* **2016**, *121*, 411–422, 449. [CrossRef]
45. Huang, Y.Y.; Zhang, S.D.; Yi, F.; Huang, C.M.; Huang, K.M.; Gan, Q.; Gong, Y. Global climatological variability of quasi-two-day waves revealed by TIMED/SABER observations. *Ann. Geophys.* **2013**, *31*, 1061–1075. [CrossRef]
46. Gu, S.-Y.; Li, T.; Dou, X.; Wu, Q.; Mlynczak, M.G.; Russell Iii, J.M. Observations of Quasi-Two-Day wave by TIMED/SABER and TIMED/TIDI. *J. Geophys. Res. Atmos.* **2013**, *118*, 1624–1639. [CrossRef]